Perforation of Aluminium Alloy-CFRP Bilayer Plates under Quasi-static and Impact Loading

B. Yu [ab], V. S. Deshpande [a], N. A. Fleck [a] [1]

[a] *Department of Engineering, University of Cambridge, Trumpington St., Cambridge, CB2 1PZ, UK*

[b] *Department of Material Science and Engineering, University of Toronto, 184 College St., Toronto, Ontario, M5S 3E4, Canada*

Abstract

The ability of a metallic surface layer to protect CFRP cross-ply plates against perforation is explored. Aluminium alloy plates (either AA1050A or AA6082-T6) were placed in front of a CFRP layer, and the bilayer was subjected to either quasi-static indentation or to ballistic impact by a spherical projectile, with rigid back support or an edge-clamped boundary condition. The observed perforation mechanism of the CFRP layer is neither influenced by the presence of the metallic layer nor by the choice of loading rate (i.e. quasi-static versus ballistic). In the back-supported condition, the CFRP layers fail by an indirect tension mode that consists of tensile failure of plies in the material directly beneath the indenter or projectile. Alternatively, in the edge-clamped condition, the CFRP layers fail by a shear plugging mechanism. Although the presence of metallic layers does not suppress the shear plugging of the underlying CFRP layer, the loaded area in the CFRP layer increases by the addition of the protective metallic layer, thereby increasing the perforation resistance of the CFRP layer.

Keywords: multi-layer composites, perforation mechanisms, quasi-static indentation, ballistics, shear plugging, indirect tension

[1] Corresponding author. Tel.: +44-1223-748240; fax: +44-1223-332662. E-mail address: naf1@eng.cam.ac.uk

1 Introduction

Carbon fibre reinforced plastic (CFRP) composites are increasingly used for structural applications due to their high stiffness and strength-to-weight ratios. Applications range from the structural frame and panels of automobiles and aircraft to fan blades for gas turbines. However, CFRP has an inferior impact resistance to composites such as ultrahigh molecular weight polyethylene (UHMWPE) fibre-based Dyneema® laminates. The high impact resistance of Dyneema® cross-ply laminates can be traced to its failure mechanism of indirect tension [1–5]. In contrast, under ballistic loading, conventional CFRP laminates of high matrix shear strength fail by a shear plugging mode (involving matrix crack formation, ply delamination, and fibre fracture) [6–8], and consequently have inferior ballistic resistance. If a strategy can be developed whereby CFRP fails by indirect tension rather than by shear plugging, then a major advance could be made in terms of its penetration resistance. Recently, it has been shown that the indirect tension mechanism can be activated in CFRP cross-ply laminates under quasi-static out-of-plane compressive loading [9], indentation loading [10], and ballistic impact loading [10]. The ballistic limit (i.e. penetration velocity) of CFRP cross-ply laminates is increased by suppressing the shear plugging mode and by activating the indirect tension mode through the reduction of matrix shear strength. The aim of the current study is to explore the possibility of improving the impact resistance of CFRP laminates by activating the indirect tension mechanism without a reduction in matrix shear strength. A possible strategy is to place a protective metallic layer in front of the laminate and thereby reduce the level of contact stress both for quasi-static indentation (as in automobile impact) and for ballistic impact, for example in the protection of lightweight armor-clad vehicles. This is the motivation for the current study.

An established method of increasing the impact resistance of long fibre composites is to add metallic interlayers, for example by alternating layers of fibre composite and aluminium alloy, the so-called fibre-metal laminate [11–16]. Currently, the most common types of fibre-metal laminate are glass reinforced aluminium laminates (GLARE®), aramid fibre reinforced aluminium laminates (ARALL®), and carbon fibre reinforced aluminium laminates (CARAL).

The failure mechanism of the fibre-metal laminates under impact loading is complex as it involves both matrix and fibre failure in the composite layer, plastic deformation of the metallic layer, and debonding at the metal-composite interface [17]. While many researchers have focused on the mechanics of GLARE® [18–22] and ARALL® [18,19,23–25], a relatively limited amount of literature is available on the impact mechanics of CARAL [13,14,16]. A recent study by Bieniaś et al. [14] investigated the damage mechanism of a composite sandwich consisting of a CFRP core and aluminium alloy face sheets, subjected to a low-velocity impact. They observed that the damage comprises transverse matrix cracks and ply delamination in the CFRP layer, plastic deformation of the aluminium alloy layers, and debonding of the metal-CFRP interfaces. Furthermore, the presence of the metallic layers reduces the extent of matrix cracking and delamination within the CFRP layer compared to that of monolithic CFRP of identical thickness. However, their study did not investigate perforation involving fibre failure at higher impact velocities. Thus, it remains unclear whether the presence of a protective metallic layer can activate the indirect tension mechanism in the CFRP layer at impact velocities near the ballistic limit of CFRP. To resolve this question, the effect of protective metallic layers on the perforation mechanism and the ballistic resistance of aluminium alloy/CFRP bilayer plates is explored herein.

Scope of Study

The objective of the current study is to determine the degree of protection by an aluminium alloy layer on the impact resistance and perforation mechanism of a CFRP plate. Figure 1 illustrates the general problem. An aluminium alloy layer is placed in front of a CFRP cross-ply laminate, thereby creating an aluminium alloy-CFRP bilayer plate. The bilayer plates are subjected to quasi-static indentation and ballistic impact by a spherical indenter or projectile under two types of support condition: a rigid back support (simulating a thick laminate) and edge-clamped. In total, four types of tests were conducted: (i) quasi-static indentation with rigid back support, (ii) quasi-static indentation test with edge-clamping, (iii) ballistic test with rigid back support, and (iv) ballistic test with edge-clamping. Two grades of aluminium alloy were used in the fabrication of the bilayer plates: (i) AA1050A-H6 and (ii) AA6082-T6. The quasi-static and ballistic performance of the bilayer plates were compared with the unprotected monolithic CFRP plate. The majority of the bilayers had no bonding of the metal/CFRP interface. However, to gain insight into the role of bonding, samples with and without adhesive were compared in selected tests.

2 Specimen Manufacture

Cross-ply laminates $[0°/90°]_{16}$ were made from Hexply® 8552/35%134/IM7 carbon fibre/epoxy prepregs (of ply thickness 0.131 mm). They were cured in an autoclave following the procedure as recommended by the Hexcel Corporation [26]. Three classes of composite plate were manufactured by making use of the cured CFRP: a monolithic CFRP plate, or by placing a single aluminium alloy sheet, AA1050A-H6 (40 Vickers) or AA6082-T6 (120 Vickers), in front of the CFRP plates. The monolithic CFRP plates were made by cutting the as-cured CFRP laminates using a diamond saw into squares of dimension $w \times w$ (where w = 75 mm, thickness = 4 mm, and an areal density of 6.28 kg/m^2). The tensile properties of the aluminum alloy sheets were measured by uniaxial tensile tests using standard dog-bone shaped specimens and a strain rate of 10^{-3}s^{-1}. The AA1050A-H6 has a 0.2% offset yield strength σ_y of 107 MPa, an ultimate tensile strength (UTS) of 117 MPa, and elongation to failure of 7%. In contrast, the AA6082-T6 has σ_y = 262 MPa, UTS = 303 MPa, and an elongation to failure of 16%, see Figure 2.

The aluminium alloy sheets were also cut into squares of in-plane dimension $w \times w$ (where w = 75 mm, thickness h = 1.5 mm, and an areal density of 3.45 kg/m^2). The following labelling procedure is used throughout this study for each group of specimens: (A) monolithic CFRP panels, (B) bilayer panels with an AA1050A-H6 sheet in front of CFRP, and (C) bilayer panels with an AA6082-T6 sheet in front of CFRP. Each monolithic plate (A) had a thickness of H = 4 mm and an areal density ρ_A of 6.28 kg/m^2 while the bilayer plates (B) and (C) each had a total thickness of 5.5 mm and an areal density ρ_A of 9.73 kg/m^2; these parameters are summarised in Table 1.

Unless otherwise specified, the bilayer plates (B) and (C) contained no adhesive between the aluminium alloy layer and the CFRP layer. This allowed for the placement of pressure sensitive films between the alloy and the CFRP layer in order to measure the contact pressure during indentation tests. The effect of a bonding between metallic layer and underlying CFRP plate on the penetration mechanism was determined by the application of an epoxy adhesive[1], Redux 810

[1] The adhesive was applied between the metal and the composite layers. The layers were then bonded under a pressure of 22 kPa for 5 hours at room temperature, and the bilayer plates were allowed to cure for a further 120 hours at room temperature to attain the fully cured state.

® to a selective set of specimens, followed by quasi-static indentation tests under an edge-clamped condition.

3 Test Methods

3.1 Ballistic Tests

Composite plates (A) and bilayer plates (B) and (C) were subjected to ballistic impact by a hardened steel ball bearing of diameter D = 5.6 mm and a mass $m_p = 7.2\times10^{-4}$ kg. (For the bilayer plates, the aluminium alloy sheet is on the front face of the plate.) Spherical projectiles were launched using a gas gun (with helium or nitrogen compressed gas, depending upn the desired velocity) with a 4.5 m long aluminium barrel having a bore diameter of 6 mm. The projectile impacted the specimens normally and centrally at an impact velocity v_0 from 30 m/s to 380 m/s, as measured using a set of laser gates placed near the exit of the barrel. High-speed images were taken using a Phantom® V1610 camera (with an inter-frame time of 16 μs and an exposure time of 0.43 μs) to record the rebound velocity v_r and to confirm the laser measurements of the impact velocity v_0. The ballistic tests were performed for two choices of boundary condition: (i) edge-clamped and (ii) back-supported, as follows.

(i) *Edge-clamped tests.* The composite plates were friction-clamped between two 12.7 mm thick steel plates using M6 bolts each with 8 Nm torque, as illustrated in Figure 3a. To achieve this, the front and back plates were surface-roughened by sand blasting. The front and backing plates each consisted of 12 equi-spaced holes (with hole diameter of 6 mm and pitch diameter of 90 mm) and a concentric opening window of diameter of D_s = 55 mm that allowed for the back face deflection and perforation of the specimens. The backing plate was mounted onto an outer frame allowing a projectile to impact the specimen normally through the centre of the opening.

(ii) *Back-supported tests*. The composite plates were placed in front of a hardened silver steel (560 Vickers) backing plate of thickness 45 mm. The projectile impacted normally and centrally in the negative z-direction as defined in Figure 3b. The specimens were loosely adhered to the backing plate using double-sided adhesive tape.

3.2 Quasi-static Indentation Tests

Composite plates (A) to (C) were subjected to out-of-plane indentation by a hemispherical indenter made of hardened silver steel (700 Vickers) with a diameter of D = 5.6 mm under (i) an edge-clamped condition and (ii) a back-supported condition. With the exception of the indenter, the specimen dimensions and the test set-up of the indentation test were identical to those in the ballistic test as shown in Figures 3a and 3b. A displacement rate $\dot{u}_z = 1.7 \times 10^{-4}\,\mathrm{m/s}$ was applied in the out-of-plane direction via a screw-driven test machine. The indentation load F was recorded by the machine load cell and the displacement of the indenter u_z was measured using ac[1].

For selected samples, the contact area of the CFRP layer (i.e. the contact area of the top face in the monolithic plates, the contact area between the aluminium alloy layer and the CFRP in the bilayer plates) and the average contact pressure were measured during the interrupted indentation tests by placing pressure measurement films[2] on top of the CFRP layer for each incremental displacement level. The pressure sensitive film contains microcapsules with various sizes and wall strengths that are correlated with pressure. The microcapsules break when a pressure of above 35 MPa is applied, creating a red coloured patch. The MS films were employed to measure the contact radius a in order to calculate the average pressure $\bar{p}$ in the subsequent interrupted tests. During the interrupted tests, a layer of MS film (of thickness $90\ \mu\mathrm{m}$) was placed on top of the CFRP layer (i.e. on top of the monolithic CFRP plate (A) or between the CFRP layer and the aluminium alloy layer of the bilayer plates (B) and (C). The contact radius a was estimated to be the radius at which the contact pressure exceeded the lower limit of the calibrated pressure range (i.e. 35 MPa). At a sufficiently high indentation displacement, the indenter penetrated both the pressure film and the CFRP layer and thus the contact radius was assumed to equal the indenter radius (i.e. $a = R$).

[1] The laser extensometer (EIR LE-05, manufactured by the Electronic Instrument Research) was operated at a scan frequency of 100 Hz.

[2] Fuji Prescale® MS. Fujifilm Holdings Corporation, 7-3, Akasaka 9-chome, Minato-ku, Tokyo 107-0052, Japan

4 Results

4.1 Failure Mechanism

As-tested specimens were sectioned across the impact zone along the fibre direction in the top ply, using an abrasive cut-off wheel. Examples of the cross-sectional microscopy images of materials (A) and (C) are shown in Figures 4 and 5, respectively. The failure mechanism of the CFRP layer depended on the imposed boundary condition (i.e. back-supported versus edge-clamped) but was neither affected by the presence of the metallic layer nor by the loading rate (quasi-static versus ballistic). In the back-supported condition, the CFRP layers failed by an indirect tension mode consisting of tensile failure of plies in the material directly beneath, and near the center line of, the indenter/projectile. In contrast, for the edge-clamped case, the CFRP layers failed by a shear plugging mechanism consisting of matrix shear cracks, ply delamination, and fibre fracture at the edge of contact. Note that, in the case of the edge-clamped condition, material (A) has a lower perforation resistance than material (C) for a given level of threat. Thus, material (C) shows a lower level of damage (i.e. a lower number of plies with fibre failure). However, the location of fibre failure in both material (A) and material (C) can easily be identified to be at the edge of contact. At a higher level of threat, more plies in material (C) would show fibre failure and its fractography would appear more similar to that of material (A) (see example in Fig. 10d).

4.2 Quasi-static Edge-clamped Indentation

The indentation response (in terms of load F versus displacement u_z) of the monolithic CFRP and of the bilayer plates are presented in Figure 6a for an edge-clamped boundary condition. All specimens exhibited an initial peak load F_i at u_z of 1-2 mm, and for illustrative purposes this point is labelled (i) for the monolithic CFRP (A). The CFRP plate (A) showed the lowest value of F_i, followed by the bilayer plate (B) and then the bilayer plates (C). Post-test inspection revealed that the initial peak load F_i was associated with matrix shear crack formation in the area beneath the edge of contact, while the fibres remained intact. Beyond the initial peak load, the indentation load increased up to a displacement of u_z of 4 mm, as labelled by point (ii) in the figure for the CFRP plate (A), again for illustration. Beyond this displacement, the indentation load began to fall in a series of dynamic events, indicating a series of failures in the CFRP layer. Post-test inspection revealed that the spikes in load were associated with fibre fracture beneath the edge of contact, as membrane tension develops within the stretched plate.

At any given stage of indentation, write a as the contact radius, and write h as the height of the aluminium layer (h = 1.5 mm), H as the height of the CFRP layer (H = 4 mm), τ_{Al} as shear yield strength of the aluminium alloy layer (taken to be $\sigma_y / 2$ of the aluminium alloy), and $\bar{\tau}$ as the average shear stress of the CFRP layer beneath the circumference of the contact area. Then, the indentation force F required to produce shear failure of the matrix in the CFRP layer of the bilayer plate, at the edge of the contact, can be estimated as:

$$F = 2\pi a\left(h\tau_{Al} + H\bar{\tau}\right) \tag{1}$$

Rearrangement of (1) gives $\bar{\tau}$ in terms of load F such that:

$$\bar{\tau} = \frac{F}{2\pi aH} - \frac{h\tau_{Al}}{H} \tag{2}$$

Recall that the contact radius a on the top face of the CFRP layer was measured during the interrupted indentation tests by placing a Prescale® film on top of the CFRP layer for each incremental displacement level (at least 17 levels for each material). The measurements of the contact radius are summarised in Figure 6b by plotting a / R (the radius of the indenter is R = 2.8 mm) as a function of displacement u_z. Upon making use of the measured values of a, the normalised average shear stresses $\bar{\tau} / \tau_y$ (where τ_y is defined to be the short beam shear strength of the CFRP layer, i.e. 99 MPa) is obtained via (2) and is plotted as a function of versus u_z in Figure 6c for materials (A) to (C). Consider first the composite plate (A). Note that damage initiation occurred at $\bar{\tau} / \tau_y$ ~1 due to matrix shear failure (i.e. when the average shear stress reached the shear strength of the CFRP layer), as labelled (i) in the figure. As the displacement increased to u_z = 4 mm, the normalised average shear stress of $\bar{\tau} / \tau_y$ exceeded unity and fibre fracture occurred beneath the edge of contact, as labelled by point (ii). We conclude that for an indent depth on the order of the ply thickness (4 mm), tensile membrane stresses develop, and failure involves the tensile fracture of the fibres contributes to the indentation strength of the CFRP and so the average shear stress exceeds unity. A similar characteristic is observed for the bilayer plates: shear failure occurs, and is followed by a more complex failure mode involving membrane tension at larger indent depths.

4.3 Quasi-static, Back-supported Indentation

The indentation responses (in terms of load F versus displacement u_z) of the composite plate (A) and bilayer plates (B) and (C) are presented in Figure 7a for the back-supported condition. Monolithic material (A) exhibited an initial peak load F_i = 14.7 kN at displacement u_z ~ 0.8 mm, as labelled (i) in Figure 7a. In contrast, specimens types (B) and (C) yielded at a displacement u_z ~ 1-2 mm due to plastic deformation of the aluminium alloy layers, delaying the peak loads F_i to u_z ~ 2.5 mm. Their initial peak loads were higher than for material (A), with material (B) at F_i = 22.2 kN and material (C) at F_i = 25.3 kN. Post-test inspection revealed that the initial peak load F_i for all 3 materials (A) to (C) was associated with fibre tensile failure of the top ply in the zone directly beneath and near the centre line of the indenter.

The average indentation pressure $\bar{p}$ beneath the indenter can be expressed as:

$$\bar{p} = \frac{F}{\pi a^2} \tag{3}$$

where the contact radius a on the top face of the CFRP layer, as measured using Prescale® films, is plotted in Figure 7b. The normalised average pressure $\bar{p}/\bar{p}_f$ (where $\bar{p}_f$ = 1350 MPa is defined to be the out-of-plane compressive strength of the CFRP layer) is plotted as a function of displacement u_z in Figure 7c. For specimens tested with back-support, damage occurred at $\bar{p}/\bar{p}_f$ ~ 1 as a result of out-of-plane compressive failure. For illustration, this is labelled (i) for the monolithic CFRP plate (A). Recall that the out-of-plane compressive strength $\bar{p}_f$ of the CFRP layer was associated with an indirect tension mechanism (as mentioned in our recent studies [9,10]), and it is concluded that the CFRP layer and bilayer plates also failed by indirect tension when indented under back-support. The presence of the aluminium face layer leads to reduced contact pressures on the CFRP layer at small values of indent depth (less than 2 mm), and to a delay in the triggering of failure of the CFRP by the indirect tension mechanism.

4.4 Effect of Boundary Condition on the Average Indentation Pressure

The average indentation pressure of composite plates under edge-clamped and back-supported conditions are compared in Figure 8 (with data for material (B) omitted for the sake of clarity and brevity). Recall that the back-supported CFRP layer for the monolithic case (A) and for the bilayer case (C) failed by the indirect tension mechanism when $\bar{p} / \bar{p}_f$ is on the order of unity. At small indent depths, the aluminium face sheet of bilayer (C) yields at $\bar{p} / \bar{p}_f$ below unity, thereby protecting the underlying CFRP layer. Now consider the edge-clamped cases (A) and (C). The CFRP failed by a shear plugging mechanism at an average pressure $\bar{p} / \bar{p}_f$ that is significantly below unity, and the indirect tension mechanism is not triggered.

4.5 Effect of the presence of a Metallic Layer on the Indentation Cut Fraction

The level of damage in the CFRP layer can be represented by the fraction of plies that exhibited fibre failure f (referred to as cut fraction). To determine f, all materials were tested at different levels of ballistic/indentation threat, with a minimum of four tests per material. The tested specimens were sectioned across the impact zone along the fibre direction in the top ply, using an abrasive cut-off wheel. The level of damage for each material was then examined through optical fractography (see example in Fig. 4 and 5 where the number of failed plies in the CFRP can be counted by observing the micrographs). Note that in the quasi-static experiments, the load-displacement responses from the repeated tests overlap one another for each material, demonstrating that the results presented here are repeatable (the data are omitted for the sake of brevity). Figure 9 compares the level of damage in the CFRP layer prior to and following the addition of a protective metallic layer, by plotting f against the indentation load F. Under an edge-clamped condition, f is defined to be the fraction of plies where fibre tensile failure was observed. Under a back-supported condition, f is defined to be the fraction of plies where fibre shear cutting was observed. Figure 9 shows that the indentation loads required to cause the same degree of damage were consistently higher for CFRP protected by a metallic layer. The resistance to damage increased in the following order: material (A), material (B), and material (C). The interrupted tests revealed that plastic deformation of the metallic layer relieves the pressure in the underlying CFRP. As a result, a larger indentation load F is required to achieve the same level of damage as for unprotected CFRP.

4.6 Effect of Adhesive bonding on Indentation Response

What is the effect of bonding face sheet to the underlying CFRP laminate? To address this, repeat indentation tests were performed on bilayer plates in the edge-clamped condition, with the 2 layers bonded by the epoxy adhesive, Redux 810®. The results are summarised in Figures 10a and 10b. Although the indentation load F required to cause a given degree of damage f (i.e. fraction of plies for which fibre tensile failure was observed) is, in general, higher for the adhesively bonded bilayer, the overall indentation responses (in terms of load F versus displacement u_z) is relatively insensitive to the presence of the adhesive layer. Furthermore, the cross-sectional microscopy images of the tested bilayer plates (B) and (C) with adhesive present showed signs of shear plugging (along with adhesive debonding at the metal/CFRP interface), see Figures 10c and 10d. Note that multiple researchers [14,16,20,27,28] have reported such debonding in fibre metal laminates when tested under impact loading and this issue is currently an ongoing research challenge in the manufacture of fibre metal laminates [29–32].

It is concluded that the presence of the adhesive leads to a detectable increase in perforation resistance, but has no influence on the failure mechanism of the bilayer materials in the edge-clamped indentation tests. Within the scope of the current study, the presence of adhesive does not promote the activation of the indirect tension mechanism. Consequently, the remaining experiments in this study were conducted in the configuration with the adhesive absent.

4.7 Ballistic Impact

The level of damage in the CFRP layer following ballistic impact, represented by the fraction of plies that exhibited fibre failure f, is plotted as a function of impact velocity v_0 in Figure 11. For all tests, the fraction of failed plies increased progressively with impact velocity. Two critical velocities can be defined: v_{init} is the velocity at initiation of failure (defined to be the highest tested impact velocity at $f = 0$), and v_p is the penetration velocity (defined to be the lowest tested impact velocity at $f = 1$). Under both edge-clamped and back-supported boundary conditions, the ballistic resistance in terms of v_{init} and v_p increased in the following order: monolithic material (A), bilayer composite plates (B), and bilayer composite plates (C). The higher ballistic resistance of material (C) was pronounced under the edge-clamped condition, where v_p exceeded the launch velocity limit of the test set-up (380 m/s) and was estimated to be v_p ~ 400 m/s based upon extrapolation of the data.

5 Discussion

5.1 Failure Mechanisms

In both the quasi-static and the ballistic tests, the failure mechanisms of the CFRP layers in the monolithic and bilayer plates were sensitive to the boundary condition but were not affected by the presence or absence of the metallic layers.

In the edge-clamped state, transverse matrix cracks form in the CFRP when the local shear stress reached the matrix shear strength. As the indentation force or impact velocity increased, the matrix crack formation was followed by ply delamination and fibre fracture. Fibre fracture provided a failure path that connected the above-mentioned matrix cracks. This failure mode is often referred to as the shear plugging mechanism, and is commonly observed in the impact failure of conventional CFRP [6,7,33–35]. In the current study, the presence of a metallic front face did not suppress this shear plugging mode in the CFRP layer under both quasi-static and ballistic loading. Measurements of the contact area during the interrupted quasi-static indentation test confirmed that first failure in the bilayer composite plates occurred when the out-of-plane shear stress of the CFRP reached its matrix shear strength. However, the contact area measurement revealed that the plastic deformation of the metallic layer spread the indentation load over a larger area. This increased the quasi-static indentation load required for shear plug formation. In similar fashion, this load spreading effect of the metallic protection occurs under ballistic loading, thus increasing the energy required for shear plug formation and enhancing the ballistic resistance.

In the back-supported state, the CFRP cross-ply laminates fail by an indirect tension mechanism facilitated by ply tensile failure directly beneath the indenter/projectile. This failure mode is in agreement with that observed by Poe Jr. [36]. In the current study, the presence of the metallic protection did not alter the failure mode of the underlying CFRP. Nevertheless, the above-mentioned load spreading effect was also observed in the back-supported tests and increased the indentation load.

5.2 A Comparison of the Quasi-static and Ballistic Responses

The above observations indicate that the failure mechanisms of a CFRP layer are the same under both quasi-static and ballistic loading. The level of damage under different loading conditions can be compared by plotting the cut fraction of plies f in the CFRP layer as a function of energy dissipation W. The energy absorption W in the quasi-static experiments was calculated by integrating the indentation load F over the displacement u_z:

$$W = -\int_0^{u_0} F du_z \tag{4}$$

where u_0 is the maximum displacement before unloading in each interrupted test. The energy dissipation W in the ballistic tests was calculated from the different kinetic energies of the projectile before impact and after rebound:

$$W = \frac{m_p}{2}\left(v_0^2 - v_r^2\right) \tag{5}$$

where m_p is the projectile mass (7.2×10^{-4} kg), v_0 is the impact velocity, and v_r is the rebound velocity. Overall, the energy dissipation in the CFRP layer under quasi-static loading is comparable to the values from the ballistic test, see Figure 12. The disparity of the energy dissipation was larger in the edge-clamped condition; this can be attributed to the presence of stress wave propagation in the ballistic test as opposed to in the quasi-static test. In general, we expect the agreement between degree of damage and dissipated energy to break down when wave propagation and other inertial effects become significant, for example when the impact velocity is on the order of elastic (or plastic) wave speeds.

The bilayer composite plates tested in this study have a higher areal density than that of the monolithic CFRP layer. To account for the effect of additional mass on the energy absorption capability, the cut fraction of plies f in the CFRP layer is plotted as a function of specific energy absorption (W / ρ_A) in Figure 13; here, the monolithic plates (A) have ρ_A = 6.28 kg/m^2 and the bilayer plates (B) and (C) have ρ_A = 9.73 kg/m^2. We find that the presence of a metallic front face increases the static and dynamic penetration resistance on the basis of specific energy dissipation.

6 Concluding remarks

The current study explores the protection against perforation by adding a protective metallic layer to cured CFRP cross-ply laminates. The aim is to determine whether the presence of an aluminium alloy layer can suppress the commonly observed brittle shear plugging mechanism in CFRP under ballistic and quasi-static loading. For this purpose, two types of aluminium alloy-CFRP bilayers were considered: a layer of either AA1050A-T6 or AA6082-T6 was placed in front of a CFRP layer. The performance of bilayer plates was compared against that of monolithic CFRP plates without metallic protection. The composite plates were then subjected to quasi-static indentation and ballistic impact by a spherical indenter or projectile under back support or edge support. In total, four types of test were conducted: (i) quasi-static indentation test with rigid back support, (ii) quasi-static indentation test with an edge-clamped condition, (iii) ballistic test with rigid back support, and (iv) ballistic test with an edge-clamped condition.

In both quasi-static and ballistic tests, the qualitative perforation mechanism in the CFRP layers was sensitive to the boundary condition but was not affected by the presence of the metallic layers. Furthermore, bonding of the metal/CFRP interface did not alter the overall failure mechanism, but it did improve the perforation resistance of the underlying CFRP. When the specimens were tested under the edge-clamped condition, back face deflection was permitted. This caused the CFRP layers to fail by shear plugging with transverse matrix cracks, ply delamination, and fibre fracture concentrated at the circumference of the contact area.

In contrast, when the specimens were tested with back-support, the material underneath the indenter/projectile was subjected to compression. As a result, the CFRP layers failed by an indirect tension mode consisting of ply tensile failure directly beneath the indenter or the projectile, similar to the failure mode observed for CFRP cross-ply laminates when subjected to uniaxial out-of-plane compression.

The presence of the metallic layer did not alter the failure mechanism in the underlying CFRP layer, but reduced the magnitude of the indentation on the CFRP layer. Consequently, under both edge-clamped and back-supported conditions, the quasi-static strength and impact resistance of the CFRP layers increased due to the presence of the metallic layers. A greater benefit was derived by a metallic layers of higher yield strength. The impact resistance (in terms of absorbed energy per areal density) measured from all the tests generally increased in the following order: monolithic CFRP, AA1050A-H6-CFRP bilayer, and AA6082-T6-CFRP bilayer. These data suggest that the use of metallic layers of high yield strength can potentially suppress shear plugging in the CFRP laminates.

Acknowledgements

The research work was sponsored by the Office of Naval Research (ONR), U.S. (Prime Award No. N62909-14-1-N232). The raw composite materials and the autoclave manufacturing process were generously provided by Hexcel Ltd. Finally, the doctoral study of one of the authors (B. Yu) was sponsored by the Croucher Foundation and the Cambridge Commonwealth, European & International Trust.

REFERENCES

[1] Karthikeyan K, Russell BP, Fleck NA, Wadley HNG, Deshpande VS. The effect of shear strength on the ballistic response of laminated composite plates. Eur J Mech A/Solids 2013;42:35–53.

[2] Attwood JP, Khaderi SN, Karthikeyan K, Fleck NA, Omasta MR, Wadley HNG, et al. The out-of-plane compressive response of Dyneema® composites. J Mech Phys Solids 2014;70:200–26.

[3] Karthikeyan K, Russell BP. Polyethylene ballistic laminates: Failure mechanics and interface effect. Mater Des 2014;63:115–25.

[4] O'Masta MR, Crayton DH, Deshpande VS, Wadley HNG. Mechanisms of penetration in polyethylene reinforced cross-ply laminates. Int J Impact Eng 2015;86:249–64.

[5] Attwood JP, Russell BP, Wadley HNG, Deshpande VS. Mechanisms of the penetration of ultra-high molecular weight polyethylene composite beams. Int J Impact Eng 2016;93:153–65.

[6] Cantwell WJ, Morton J. Comparison of the low and high velocity impact response of CFRP. Composites 1989;20:545–51.

[7] Cantwell WJ, Morton J. Geometrical effects in the low velocity impact response of CFRP. Compos Struct 1989;12:39–59.

[8] Cantwell WJ, Morton J. Impact perforation of carbon fibre reinforced plastic. Compos Sci Technol 1990;38:119–41.

[9] Yu B, Kaderi SN, Deshpande VS, Fleck NA. The Effect of Matrix Shear Strength on the out-of-plane Compressive Strength of CFRP Cross-ply Laminates. Int J Solids Struct:Submitted.

[10] Yu B, Karthikeyan K, Deshpande VS, Fleck NA. Perforation resistance of CFRP beams to quasi-static and ballistic loading: The role of matrix strength. Int J Impact Eng 2017;108:389–401.

[11] Krull M, Vlot A, Krull M. Impact damage resistance of various fibre metal laminates. J Phys Iv 1997;7:1045–50.

[12] Lawcock G, Ye L. Effects of fibre_matrix adhesion on CARBON/FIBRE/REINFORCED METAL LAMINATES- II. Impact behaviour. Compos Sci Technol 1998;3538:1621–8.

[13] Song SH, Byun YS, Ku TW, Song WJ, Kim J, Kang BS. Experimental and numerical

investigation on impact performance of carbon reinforced aluminum laminates. J Mater Sci Technol 2010;26:327–32.

[14] Bieniaś J, Jakubczak P, Surowska B, Dragan K. Low-energy impact behaviour and damage characterization of carbon fibre reinforced polymer and aluminium hybrid laminates. Arch Civ Mech Eng 2015;15:925–32.

[15] Yu G-C, Wu L-Z, Ma L, Xiong J. Low Velocity Impact of Carbon Fiber Aluminum Laminates. Compos Struct 2015;119:757–66.

[16] Jaroslaw B, Barbara S, Patryk J. The Comparison of Low-Velocity Impact Resistance of Aluminum/Carbon and Glass Fiber Metal Laminates. Polym Compos 2016;37:1056–63.

[17] Sadighi M, Alderliesten RC, Benedictus R. Impact resistance of fiber-metal laminates: A review. Int J Impact Eng 2012;49:77–90.

[18] Vlot A. Impact properties of Fibre Metal Laminates. Compos Eng 1993;3:911–27.

[19] Vlot A, Kroon E, La Rocca G. Impact Response of Fiber Metal Laminates. Key Eng Mater 1998;141–143:235–76.

[20] Compston P, Cantwell WJ, Jones C, Jones N. Impact perforation resistance and fracture mechanisms of a thermoplastic based fiber-metal laminate. J Mater Sci Lett 2001;20:597–9.

[21] Hoo Fatt MS, Lin C, Revilock DM, Hopkins DA. Ballistic impact of GLARE fiber-metal laminates. Compos Struct 2003;61:73–88.

[22] Caprino G, Spataro G, Del Luongo S. Low-velocity impact behaviour of fibreglass-aluminium laminates. Compos Part A Appl Sci Manuf 2004;35:605–16.

[23] Johnson VVS. Impact and Residual Fatigue Behavior of ARALL and AS6/ 5245 Composite Materials October 1986. 1986.

[24] Sun CT, Dicken A, Wu HF. Characterization of impact damage in ARALL laminates. Compos Sci Technol 1993;49:139–44.

[25] Vlot A. Impact loading on fibre metal laminates. Int J Impact Eng 1996;18:291–307.

[26] Hexcel Composites. HexPly® 8552 epoxy matrix (180°C/356F curing matrix), product data. 2013.

[27] Atas C. An Experimental Investigation on the Impact Response of Fiberglass/Aluminum Composites. J Reinf Plast Compos 2007;26:1479–91.

[28] Wu G, Yang JM, Hahn HT. The impact properties and damage tolerance and of bi-

directionally reinforced fiber metal laminates. J Mater Sci 2007;42:948–57.

[29] Kim WS, Yun IH, Lee JJ, Jung HT. Evaluation of mechanical interlock effect on adhesion strength of polymermetal interfaces using micro-patterned surface topography. Int J Adhes Adhes 2010;30:408–17.

[30] Yun IH, Kim WS, Kim K, Jung JM, Lee JJ, Jung HT. Highly enhanced interfacial adhesion properties of steel-polymer composites by dot-shaped surface patterning. J Appl Phys 2011;109.

[31] Ning H, Li Y. Improvement of interlaminar mechanical properties of CARALL based on nanofiller interface reinforcement and other fabrication techniques. 13th Int. Conf. Fract. Vol 5, Beijing, China: 2013, p. 3465–75.

[32] Pärnänen T, Kanerva M, Sarlin E, Saarela O. Debonding and impact damage in stainless steel fibre metal laminates prior to metal fracture. Compos Struct 2015;119:777–86.

[33] Cristescu N, Malvern LE, Sierakowski RL. Failure Mechanisms in Composite Rates Impacted by Blunt-Ended Penetrators. Foreign Object Impact Damage to Compos A Symp 1975:No. 568 p. 159.

[34] Cantwell, W.J.; Morton J. The impact resistance of composite materials - a review. Composites 1991;22(5):347–62.

[35] Zhou G. Damage mechanisms in composite laminates impacted by a flat-ended impactor. Compos Sci Technol 1995;54:267–73.

[36] Poe Jr. CC. Simulated Impact Damage in a Thick Graphite/epoxy Laminate Using Spherical Indenters. J Reinf Plast Compos 1991;10:293–307.

FIGURE CAPTIONS

Fig. 1 An aluminium alloy-CFRP bilayer struck by a spherical indenter/projectile. All dimensions are in mm.

Fig. 2 Uniaxial tensile curves of aluminium alloy AA1050A-H6 and AA6082-T6.

Fig. 3 Sketches of (a) edge-clamped and (b) back-supported aluminium alloy-CFRP bilayer plates for impact by a spherical projectile. All dimensions are in mm.

Fig. 4 Cross-sectional images indicating that, regardless of the loading conditions, monolithic CFRP plate material (A) failed by shear plugging in the edge-clamped test and failed by indirect tension in the back-supported test.

Fig. 5 Cross-sectional images indicating that, regardless of the loading conditions, the CFRP layer of bi-material (C) failed by shear plugging in the edge-clamped test and failed by indirect tension in the back-supported test.

Fig. 6 Quasi-static indentation responses of edge-clamped plates (A) to (C). (a) load F versus displacement u_z, (b) normalised contact radius a/R versus displacement u_z, and (c) normalised average shear stress $\bar{\tau}/\tau_y$ versus displacement u_z. First failure, labelled as (i), is associated with matrix cracking whereas the second failure, labelled as (ii), denotes fibre fracture beneath the edge of contact.

Fig. 7 Quasi-static indentation responses of back-supported plates (A) to (C). (a) load F versus displacement u_z, (b) normalised contact radius a/R versus displacement u_z, and (c) normalised average pressure $\bar{p}/p_f$ versus displacement u_z. First failure, labelled (i), is associated with fibre tensile failure directly beneath the indenter.

Fig. 8 Quasi-static indentation load-displacement responses of materials (A) and (C) under edge-clamped and back-supported conditions in terms of normalised average pressure $\bar{p}/p_f$ versus displacement u_z.

Fig. 9 The indentation cut fraction f in materials (A) to (C) versus indentation load F under (a) edge-clamped and (b) back-supported conditions.

Fig. 10 Edge-clamped indentation response of bilayer material (B) and (C) with and without bonding between layers. (a) indentation load F versus u_z and (b) indentation cut fraction f

versus load F. (c)-(d) Cross-sectional micrographs of the bonded bilayer plates (B) and (C), after testing to the indentation load F levels as labeled (i) and (ii) in Figure 11b.

Fig. 11 The cut fraction f in materials (A) to (C) versus impact velocity v_0 under (a) edge-clamped and (b) back-supported conditions.

Fig. 12 Cut fraction f in materials (A) to (C) from quasi-static and dynamic tests versus energy dissipation W under (a) edge-clamped and (b) back-supported conditions.

Fig. 13 Cut fraction f in materials (A) to (C) from quasi-static and dynamic tests versus specific energy dissipation W / ρ_A under (a) edge-clamped and (b) back-supported conditions.

TABLE CAPTIONS

Table 1 Layer thickness and areal density of monolithic CFRP and the aluminium alloy-CFRP bilayer plates.

Table 1 Layer thickness and areal density of monolithic CFRP and the aluminium alloy-CFRP bilayer plates.

Material	Metal layer thickness h (mm)	CFRP layer thickness H (mm)	Total plate thickness $H+h$ (mm)	Total areal density ρ_A $\left(\mathrm{kg/m^2}\right)$
A	--	4	4	6.28
B	1.5	4	5.5	9.73
C	1.5	4	5.5	9.73

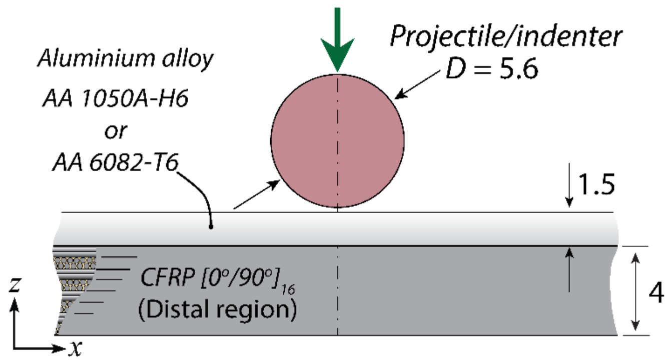

Fig. 1 An aluminium alloy-CFRP bilayer struck by a spherical indenter/projectile. All dimensions are in mm.

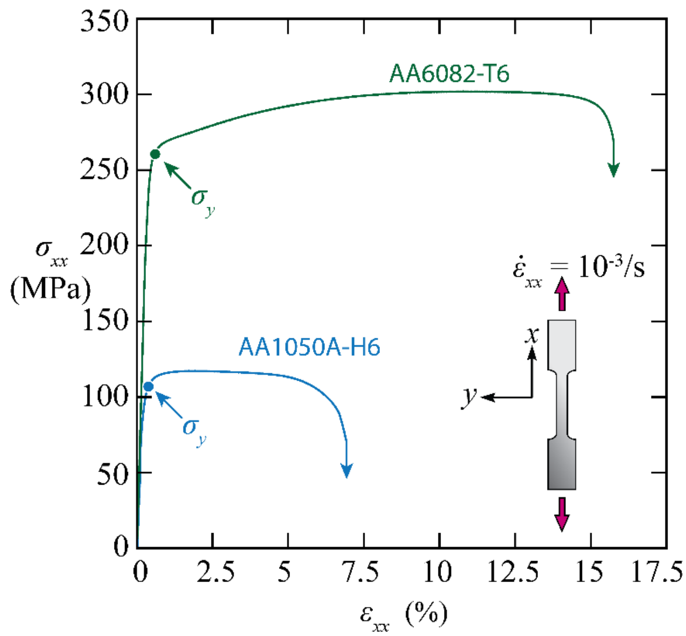

Fig. 2 Uniaxial tensile curves of aluminium alloy AA1050A-H6 and AA6082-T6.

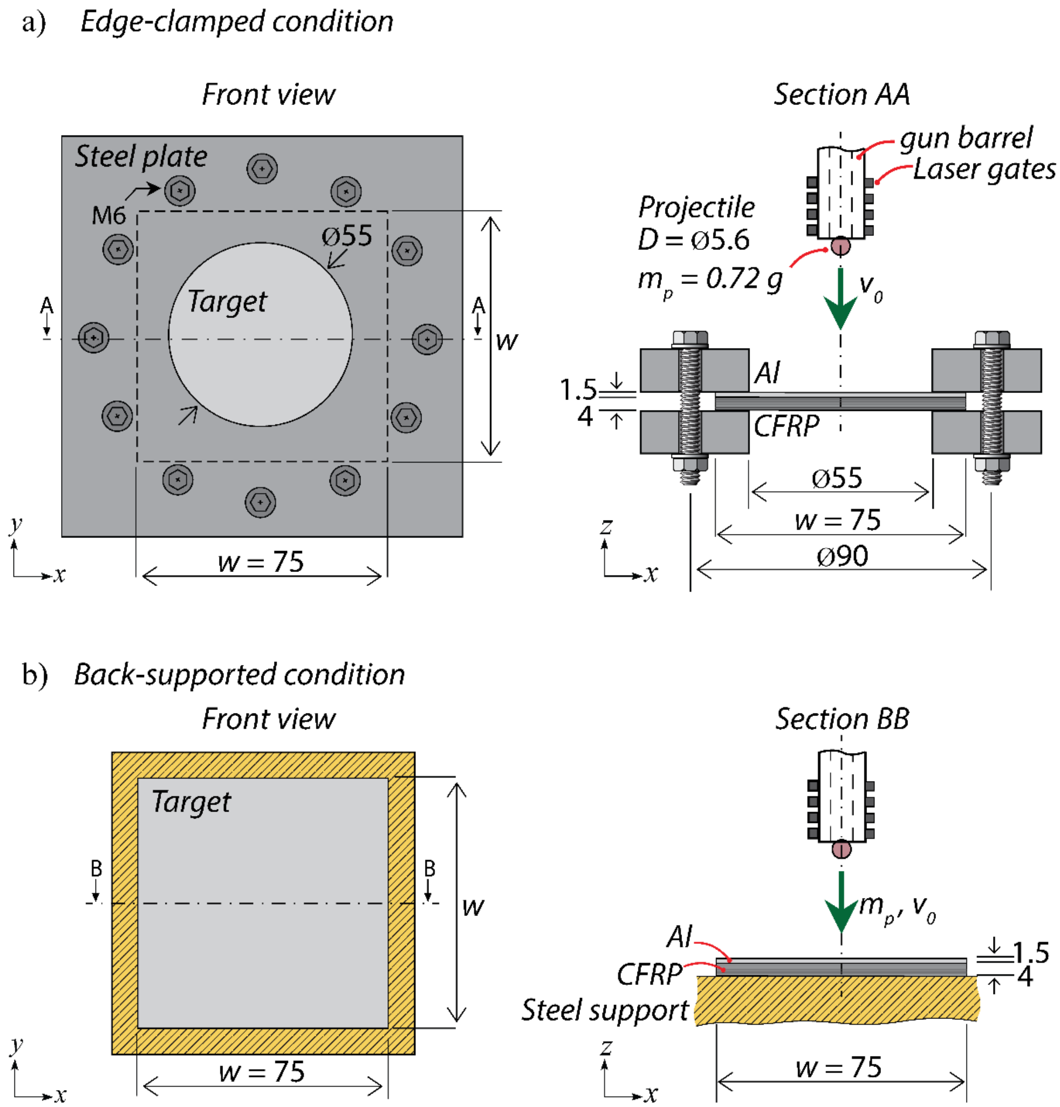

Fig. 3 Sketches of (a) edge-clamped and (b) back-supported aluminium alloy-CFRP bilayer plates for impact by a spherical projectile. All dimensions are in mm.

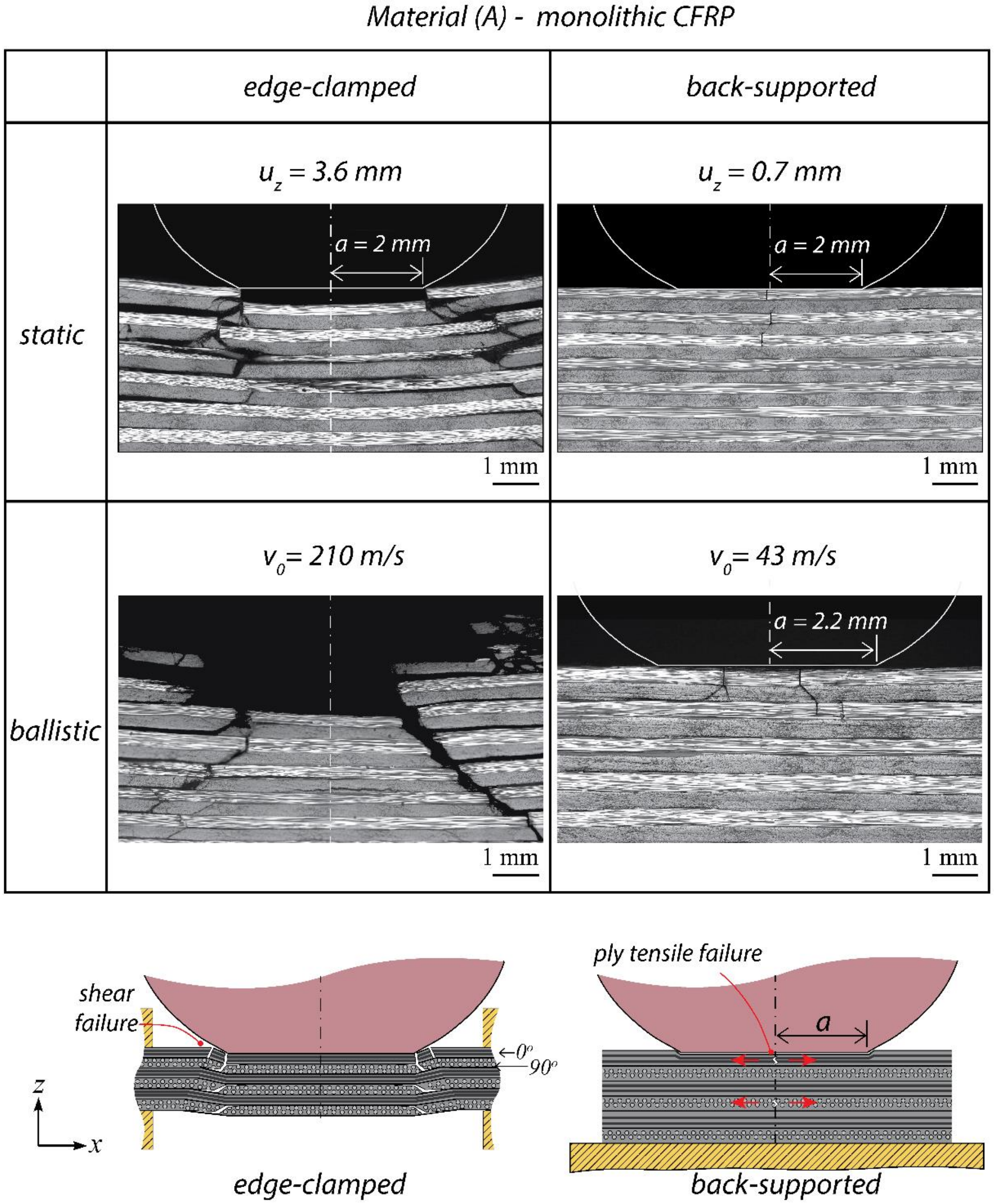

Fig. 4 Cross-sectional images indicating that, regardless of the loading conditions, monolithic CFRP plate material (A) failed by shear plugging in the edge-clamped test and failed by indirect tension in the back-supported test.

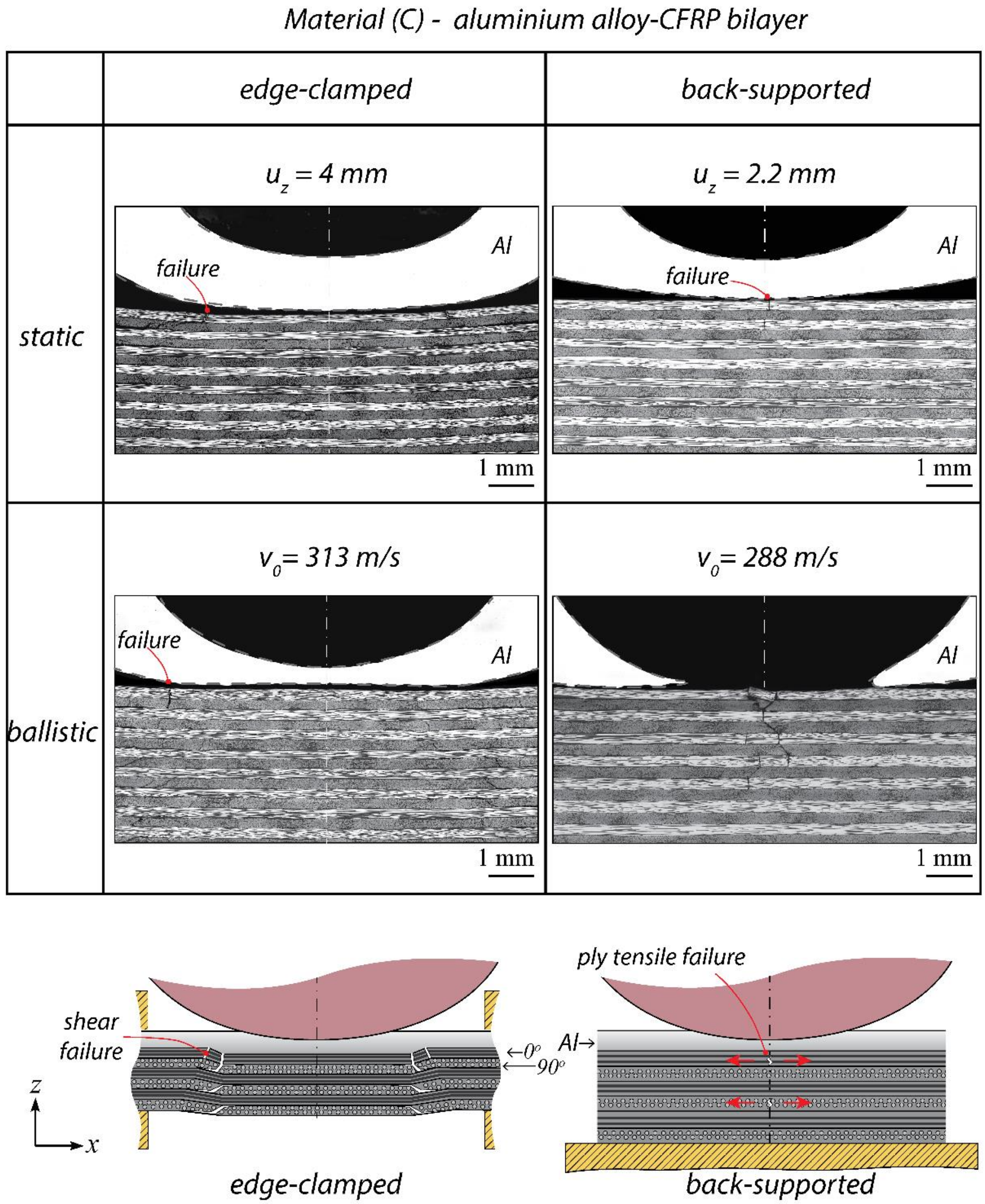

Fig. 5 Cross-sectional images indicating that, regardless of the loading conditions, the CFRP layer of bi-material (C) failed by shear plugging in the edge-clamped test and failed by indirect tension in the back-supported test..

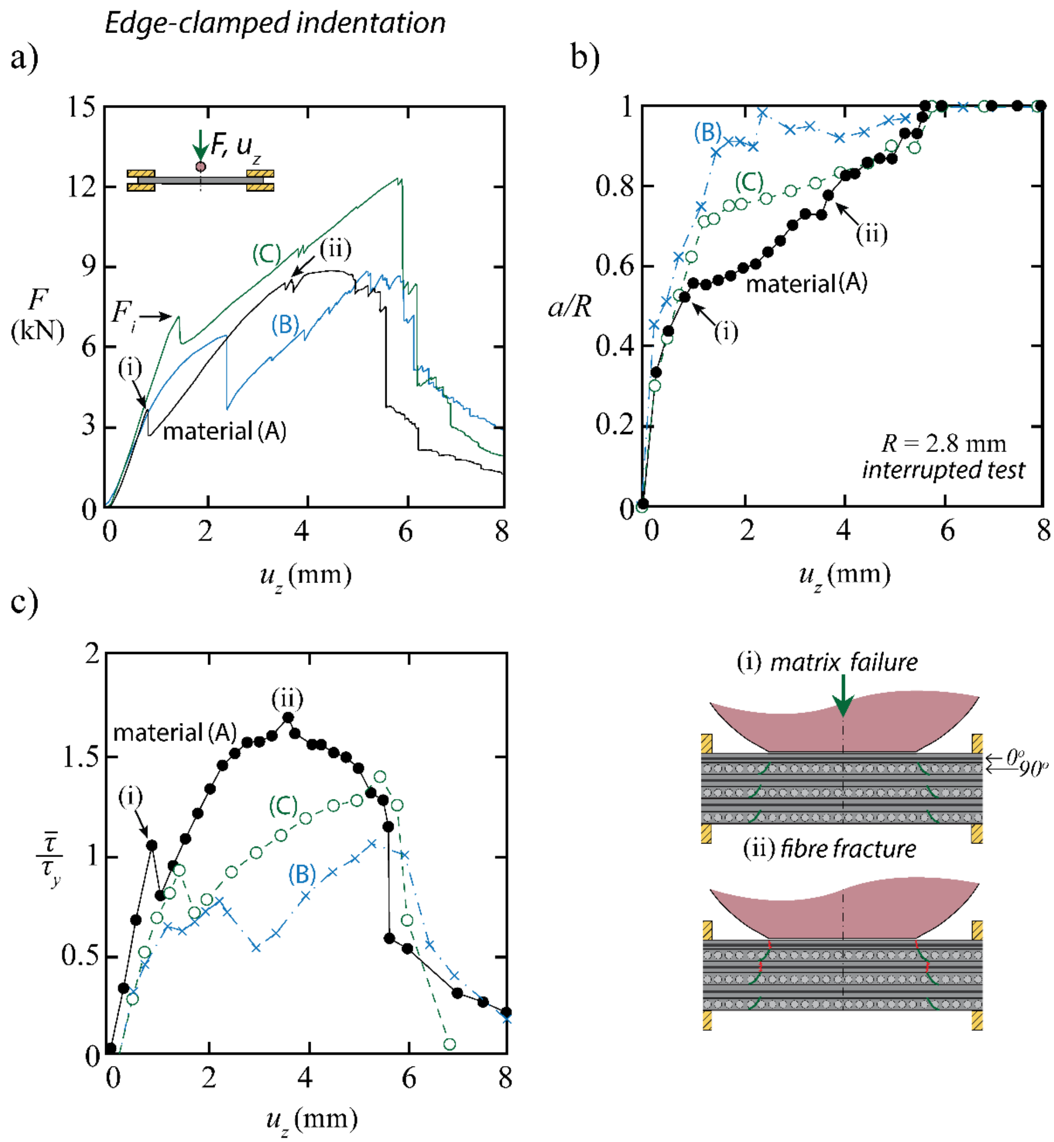

Fig. 6 Quasi-static indentation responses of edge-clamped plates (A) to (C). (a) load F versus displacement u_z, (b) normalised contact radius a/R versus displacement u_z, and (c) normalised average shear stress $\bar{\tau}/\tau_y$ versus displacement u_z. First failure, labelled as (i), is associated with matrix cracking whereas the second failure, labelled as (ii), denotes fibre fracture beneath the edge of contact.

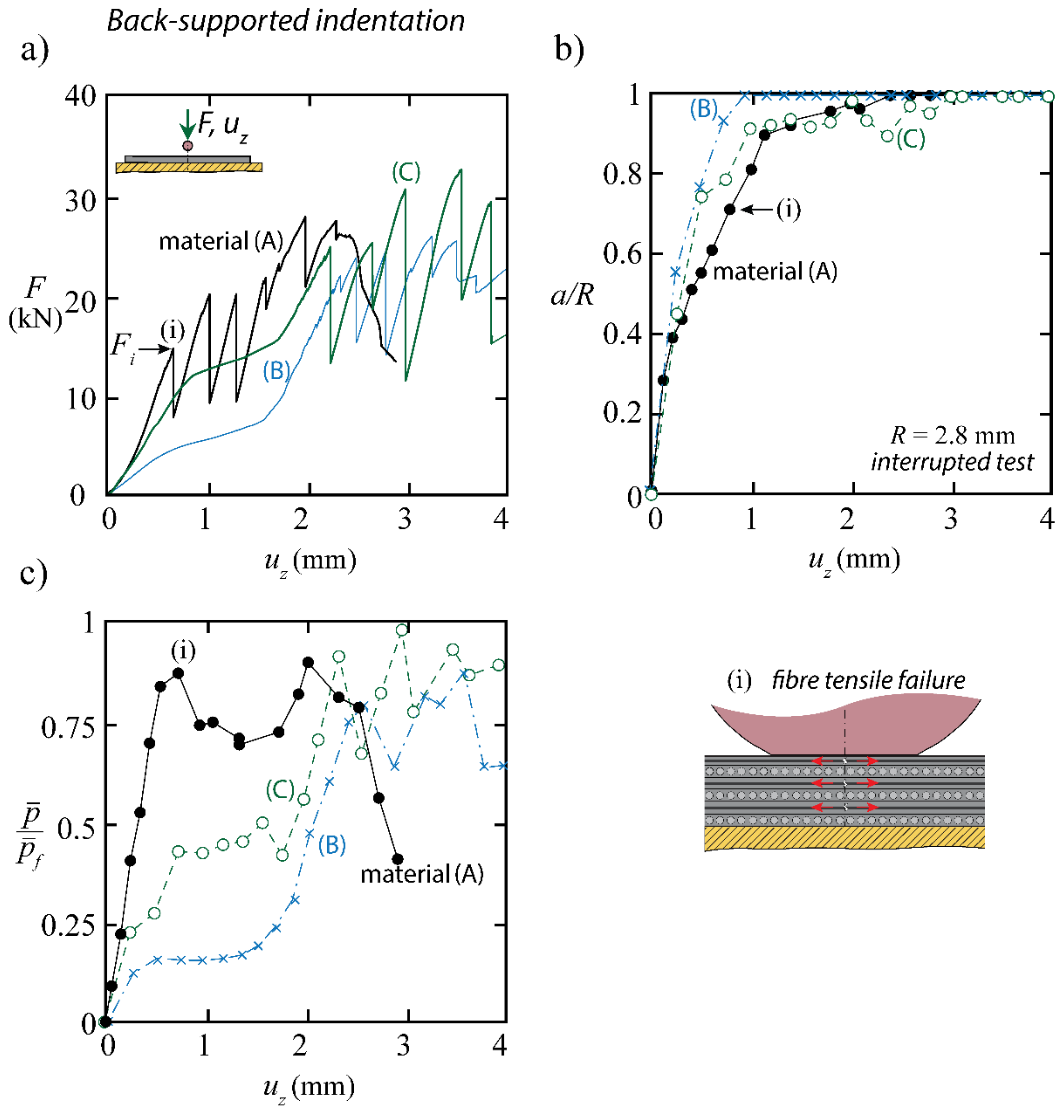

Fig. 7 Quasi-static indentation responses of back-supported plates (A) to (C). (a) load F versus displacement u_z, (b) normalised contact radius a/R versus displacement u_z, and (c) normalised average pressure $\bar{p}/p_f$ versus displacement u_z. First failure, labelled (i), is associated with fibre tensile failure directly beneath the indenter.

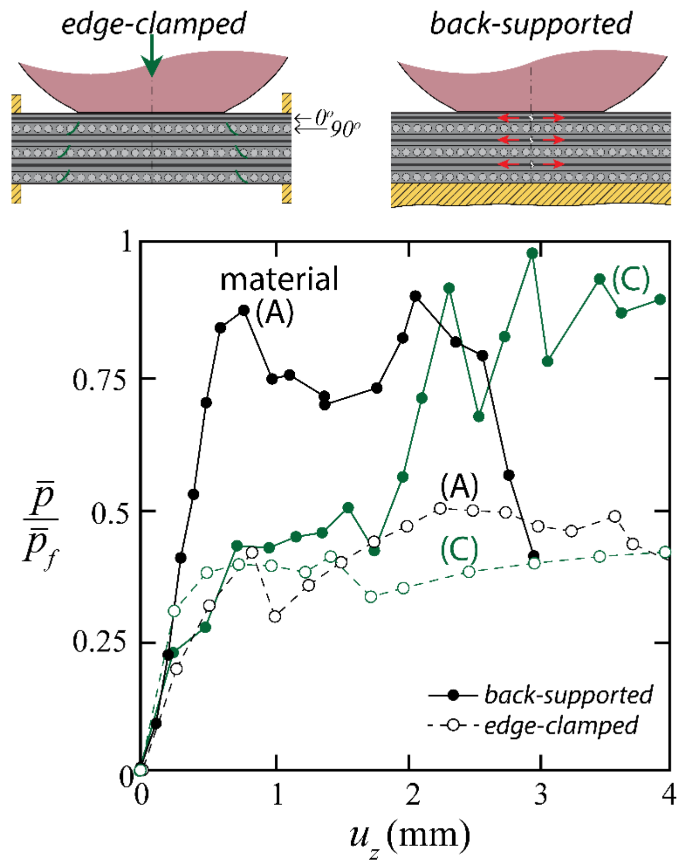

Fig. 8 Quasi-static indentation load-displacement responses of materials (A) and (C) under edge-clamped and back-supported conditions in terms of normalised average pressure $\bar{p}/p_f$ versus displacement u_z.

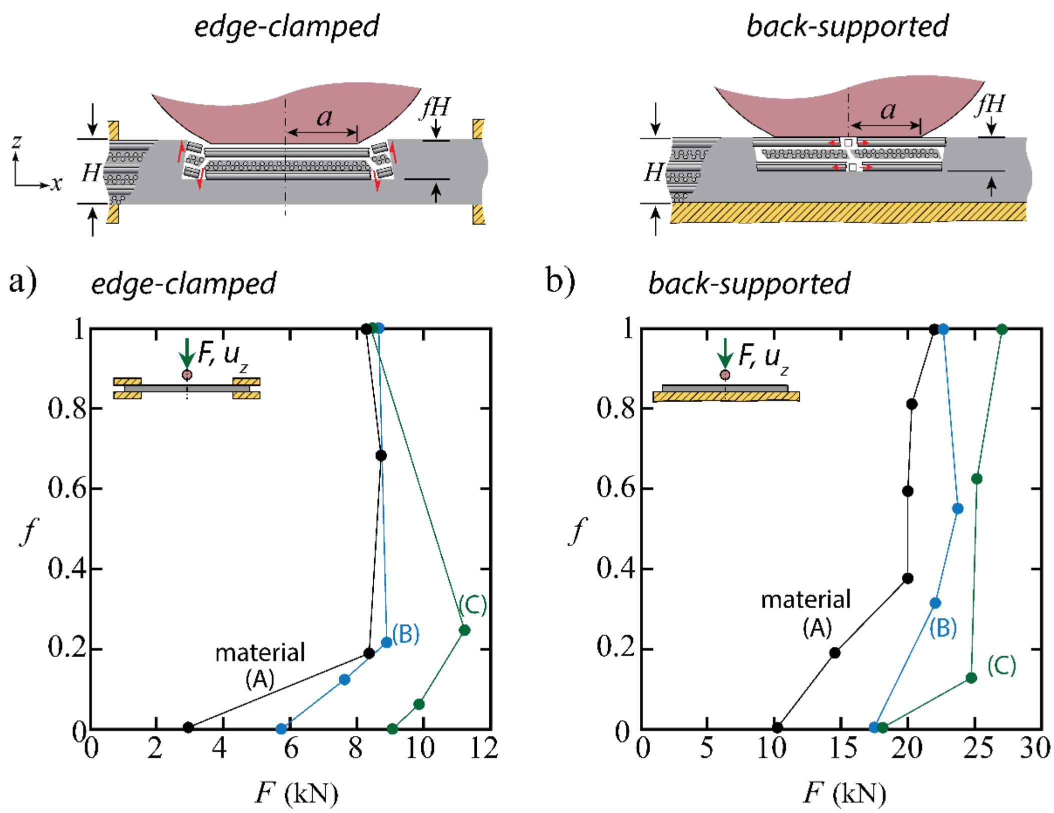

Fig. 9 The indentation cut fraction f in materials (A) to (C) versus indentation load F under (a) edge-clamped and (b) back-supported conditions.

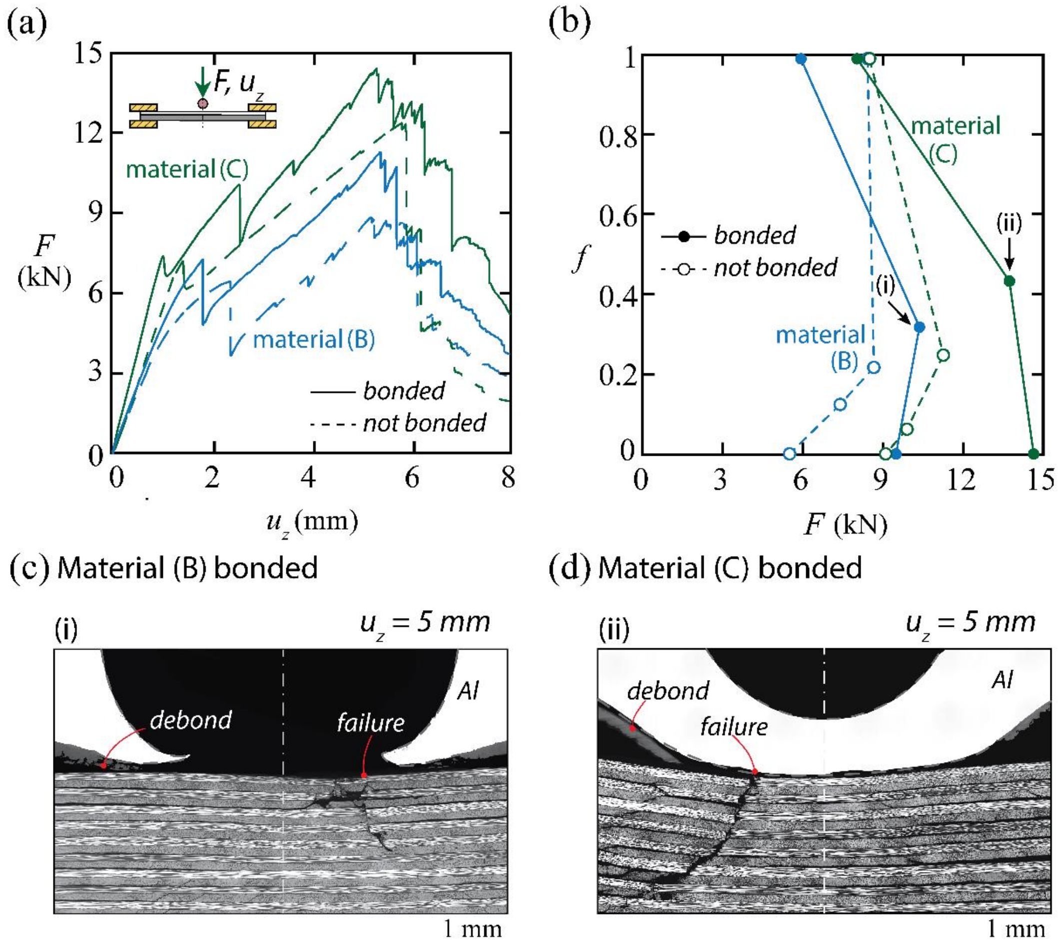

Fig. 10 Edge-clamped indentation response of bilayer material (B) and (C) with and without bonding between layers. (a) indentation load F versus u_z and (b) indentation cut fraction f versus load F. (c)-(d) Cross-sectional micrographs of the bonded bilayer plates (B) and (C), after testing to the indentation load F levels as labeled (i) and (ii) in Figure 11b.

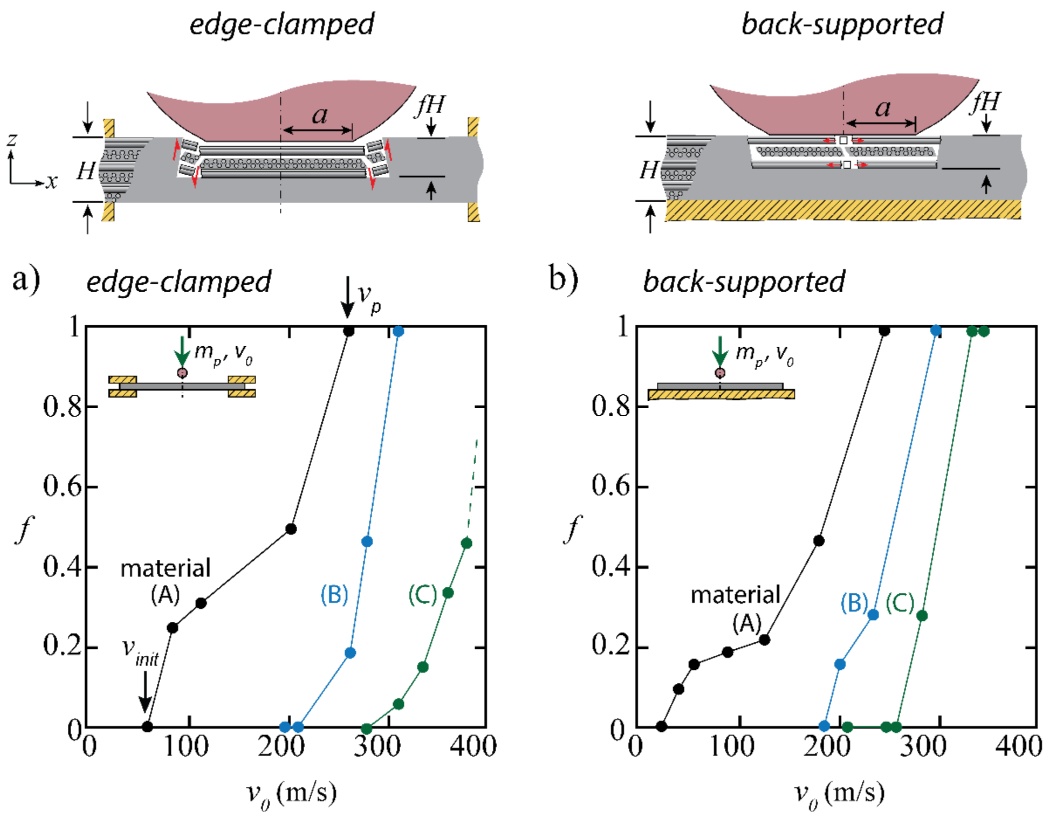

Fig. 11 The cut fraction f in materials (A) to (C) versus impact velocity v_0 under (a) edge-clamped and (b) back-supported conditions.

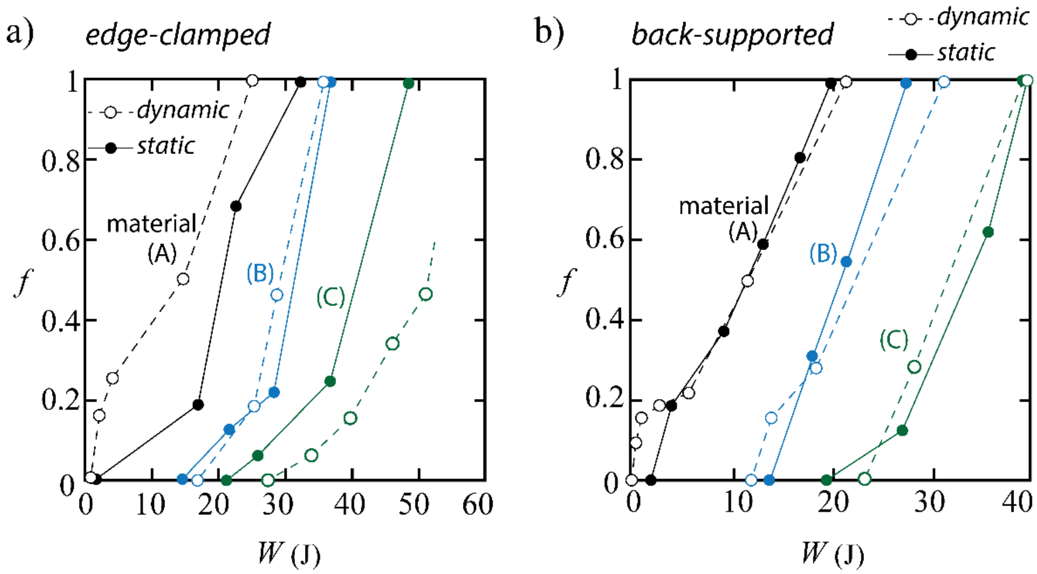

Fig. 12 Cut fraction f in materials (A) to (C) from quasi-static and dynamic tests versus energy dissipation W under (a) edge-clamped and (b) back-supported conditions.

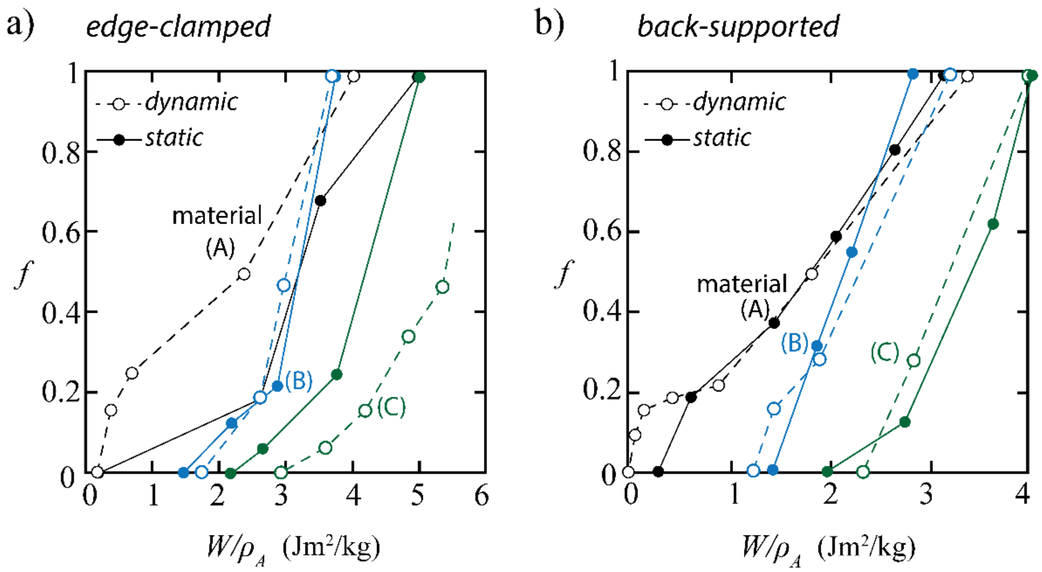

Fig. 13 Cut fraction f in materials (A) to (C) from quasi-static and dynamic tests versus specific energy dissipation W/ρ_A under (a) edge-clamped and (b) back-supported conditions.